

Axisymmetric relativistic self-channeling of laser light in plasmas

A. Kim,¹ M. Tushentsov,¹ F. Cattani,² D. Anderson,² and M. Lisak²

¹*Institute of Applied Physics, Russian Academy of Sciences, 603950 Nizhny Novgorod, Russia*

²*Department of Electromagnetics, Chalmers University of Technology, SE-412 96 Göteborg, Sweden*

(Received 13 December 2001; published 6 March 2002)

By using an improved cavitation model, relativistic self-channeling structures are derived, which make it possible to propagate laser powers exceeding the critical one for self-focusing. A propagation mode for high laser power is also presented which is qualitatively different from those in the weakly relativistic case. Structural stability analysis shows that stable self-wave-guide propagation can take place.

DOI: 10.1103/PhysRevE.65.036416

PACS number(s): 52.35.Mw, 52.38.Hb, 42.65.Wi

I. INTRODUCTION

In recent years, the combined effect of ponderomotive and relativistic nonlinearities have assumed an important role for the problem of penetration of super-intense laser pulses into underdense plasmas especially regarding self-focusing and self-channeling phenomena [1–4]. The importance of these phenomena is not only intrinsic but is also related to the requirements of most of the advanced application schemes like, e.g., inertial confinement fusion [5], where the laser radiation has to propagate over distances considerably beyond the diffraction limit without significant energy losses. Numerical and experimental studies have given evidence for the formation of stable channels and radiation filaments [6,7].

As was shown by Sun *et al.* [1], the properties of relativistic self-focusing can change drastically for very high-power beams. In this case, the laser intensity is so strong that the ponderomotive force can expel all electrons from the region of the high-intensity field. Recent studies [3,6,8–10] demonstrate that stable channeling can occur with propagating power exceeding the critical one for relativistic self-focusing [11], i.e., $P > P_{cr} = 17\omega^2/\omega_{pe}^2$ GW. The laser radiation is then confined in a self-induced waveguide, which is emptied of electrons.

The physical idea behind self-focusing and self-channeling with superintense laser pulses is that the relativistic motion acquired by the plasma electrons and the density perturbations due to the action of the laser ponderomotive force (time scales are so short that ions can be considered as immobile) can induce significant modifications in the refractive index of the plasma. Electrons tend to be expelled from the focal region of the laser beam, while acquiring relativistic quiver velocities and the pulse is focused into what in principle could be a catastrophic singularity. However, if the intensity is high enough, it has been shown that full electron cavitation occurs, leading to a stable channeling of the radiation in cavities depleted of their electrons and where consequently further focusing cannot take place. The complicated interplay between the laser action and the forces due to the charge-density perturbations makes it difficult to follow analytically such phenomena while taking rigorously into account global plasma quasineutrality. In order to make analytical progress, a simplified cavitation model has been used [1,3,6,8]. However, as was recently pointed out in [10], a

self-consistent description of the relativistic self-focusing that solves the problem of “negative electron density” without violating the total charge conservation was still missing.

In our previous work [12], we presented an improved cavitation model that, in a planar geometry, allowed for exact two-dimensional (2D) stationary analytical solutions describing the transverse structures of waveguide channels with electron cavitation. In this model both the ponderomotive and relativistic nonlinearities were taken into account, along with the constraint given by total charge conservation. It was shown that multifilament structures can be described exactly in analytical terms and the threshold power for the generation of such structures was calculated. It turned out that the threshold power was lower than what was predicted without taking into account charge conservation. The main purpose of the present paper is to find analogous stationary structures in the 3D case with axisymmetric geometry, using numerical computations and to analyze the structural stability of these solutions. As is well known, the higher dimensionality in self-focusing is very important in order to be able to deliver laser powers much higher than the critical one but also leads to fundamental differences as compared to the one-dimensional case.

In what follows, we will first introduce our model and justify the approximations we have considered in order to analyze the self-focusing and self-channeling phenomena. Then we will determine the shape of the stationary structures and calculate the power required to generate them. It will also be demonstrated how the form of the structures changes for increasing incident laser power. The central problem will then be to consider in more detail those structures that exhibit full electron cavitation and to determine exactly their properties and stability.

II. BASIC EQUATIONS

In order to identify the effect due to the action of ponderomotive and relativistic nonlinearities, we will consider the interaction between an ultrahigh power laser pulse and an underdense plasma, i.e., a plasma with $n_0 = N_0/N_{cr} < 1$, where N_0 is the unperturbed electron density and $N_{cr} = m\omega^2/4\pi e^2$ is the critical density. Introducing the different time scales as ω_{pe}^{-1} , the electron response time, ω_{pi}^{-1} , the ion response time, and ω^{-1} , the laser carrier oscillation time, the main requirements on the laser parameters are that the inten-

sity must be high enough to set electrons in relativistic quiver motion, while the characteristic time of the interaction dynamics τ must be such that

$$\omega_{pi}^{-1} \gg \tau \gg \omega_{pe}^{-1} > \omega^{-1}.$$

For relativistic electron velocities all thermal and collisional effects can be neglected and the electron thermal pressure becomes negligible compared to the ponderomotive pressure. Furthermore, the inequality $\omega_{pi}^{-1} \gg \tau$ guarantees that ion dynamics can be disregarded. In this case, we can start our analysis with the model (see also [13]) that describes a relativistic cold electron fluid with a background of immobile ions and which is based on Maxwell's equations together with the equation of motion for the electron fluid and a gauge choice (the Coulomb gauge will be adopted in our case)

$$\nabla^2 \mathbf{A} - \frac{1}{c^2} \frac{\partial^2 \mathbf{A}}{\partial t^2} = \frac{1}{c} \frac{\partial}{\partial t} \nabla \varphi + \frac{4\pi}{c} N e \mathbf{v}, \quad (1)$$

$$\nabla^2 \varphi = 4\pi e (N - N_0), \quad (2)$$

$$m \gamma \mathbf{v} = \frac{e}{c} \mathbf{A} + \nabla \psi, \quad (3)$$

$$\frac{\partial \psi}{\partial t} = e \varphi - m c^2 (\gamma - 1), \quad (4)$$

$$\nabla \cdot \mathbf{A} = 0. \quad (5)$$

Here, $\gamma = 1/\sqrt{1 - \mathbf{v}^2/c^2}$ is the relativistic factor, N is the electron density, e and m are the electron charge and mass, respectively, \mathbf{A} is the electromagnetic vector potential, φ is the electrostatic scalar potential, and ψ is a scalar function which expresses the electron canonical momentum. Equations (3) and (4) imply that we are assuming vortex-free motion of the electrons. Central to the model is the fact that the charge conservation law is contained in these equations: Taking the divergence of Eq. (1) and using Eqs. (2) and (5) we find that the charge conservation law

$$\frac{\partial N}{\partial t} + \nabla \cdot (N \mathbf{v}) = 0 \quad (6)$$

is automatically satisfied, i.e., the total charge is conserved.

The second inequality ($\tau \gg \omega_{pe}^{-1}$) will help us in isolating the combined effect of ponderomotive and relativistic nonlinearities from other effects like wake field generation, as the pulse will be long enough to disregard phenomena due to longitudinal charge separation. Given the assumptions on the characteristic time scales of the interacting pulse and the plasma, we expect that stationary plasma-field structures can emerge, as the electron fluid should have time to approach a quasisteady state. On the other hand, the question if these structures actually appear on a time scale that effectively allows us to disregard other effects and complications was in fact answered confirmatively by numerical simulations in

[10]. Finally, the inequality $\tau \gg \omega^{-1}$ will allow us to use the slowly varying envelope approximation in order to single out the fast optical time scale.

Naturally, the laser-plasma interaction will present a dynamical stage described by the full time-dependent set of equations, but the existence of quasistationary structures that can be realized as a result of the interaction and their stability are interesting and important questions. The search for quasisteady solutions leads us to an important simplification: if the electron fluid is initially vortex free, we can assume that ψ remains equal to zero. Furthermore, in the paraxial approximation, the longitudinal component of the vector potential can be neglected and we can assume $e \mathbf{A}(\mathbf{r}, t)/m c^2 = (1/2) \{a(\mathbf{r}_\perp, z) (\mathbf{e}_x + i \mathbf{e}_y) \exp[i(kz - \omega t)] + c.c.\}$, where z has been chosen as the propagation coordinate and $k = \omega/c$ is the vacuum wave number. As linear polarization would not bring any significant change into the model, we can consider, for the sake of simplicity, circularly polarized radiation. Thus, our basic equations will result in a simplified set of equations

$$2ik \frac{\partial a}{\partial z} + \nabla_\perp^2 a - \frac{k^2 n_0}{\gamma} n a = 0, \quad (7)$$

$$\nabla_\perp^2 \phi = k^2 n_0 (n - 1), \quad (8)$$

$$\phi = \gamma - 1 \quad \text{if and only if } n \neq 0, \quad (9)$$

$$\gamma = \sqrt{1 + |a|^2}, \quad (10)$$

where $\nabla_\perp^2 \equiv \partial^2/\partial x^2 + \partial^2/\partial y^2$ accounts for the diffraction in the transverse (x, y) plane and we have introduced the following normalization: $n = N/N_0$, $\phi = e\varphi/(m c^2)$. So far, our model equations are exactly analogous to those presented by Sun and others [1, 3, 8, 9], except for one point: the subsequent treatment of Eqs. (8) and (9). The delicate point is the determination of the electron density profile $n(\mathbf{r})$. As a matter of fact, $n(\mathbf{r})$ is determined by Poisson's Eq. (8) together with the force balance Eq. (9) and nothing in the model prevents $n(\mathbf{r})$ from assuming nonphysical negative values. The common way to solve this problem, suggested by the physics of the problem itself, is to set $n(\mathbf{r}) = 0$ where the equations lead to the unphysical result of negative values. This is meant to model mathematically the fact that, as soon as electrons start cavitating, the force balance equation loses its validity since in a region depleted of its electrons there are no particles left to balance the ponderomotive force. Unfortunately, setting the boundaries of the depletion region at the point where the density vanishes does not respect total charge conservation and it has been shown that this usually leads to an excess of negative charges, which in turn means that the power required to generate these structures will be overestimated [12]. It also means that the set of Eqs. (7)–(10) cannot be used for simulation by itself without additionally including the electron temperature (thermal force) as in [10] or by using a fluid model [see Eqs. (3) and (4)]. The problem is due to the fact that the cavitation boundaries within the framework of Eqs. (7)–(10) can be defined self consistently only if the global structure of the solution is determined. Nevertheless, this set of equations is useful for determining the self-

focusing structures and their stability because in this case the self-consistency problem can be overcome.

III. AXISYMMETRIC STRUCTURES

A. Self-guiding channel

First, we extend the solution presented by Sun *et al.* in order to rigorously account for total charge conservation and to use this constraint to determine the actual width of the electron cavity. Assuming a solution for the field in the form $a(\mathbf{r}_\perp, z) = a_s(r) \exp(-i\kappa z)$, we can rewrite Eqs. (7)–(10) as follows:

$$\nabla^2 a_s + \left(\kappa - \frac{n_s}{\gamma_s} \right) a_s = 0, \quad (11)$$

$$\nabla^2 \phi_s = n_s - 1, \quad (12)$$

$$\phi_s = \gamma_s - 1 \quad \text{if and only if } n_s \neq 0, \quad (13)$$

$$\gamma_s = \sqrt{1 + a_s^2}, \quad (14)$$

where κ is the propagation constant, $\nabla^2 \equiv (1/r)d(r dr/dz)/dz$ and we have used the following dimensionless variables: $r = k\sqrt{n_0}r$, $z = kn_0 z/2$.

Assuming $n_s(r) > 0$ and combining Eqs. (12) and (13) we obtain an equation describing the electron density under the effect of both the ponderomotive force and the force due to charge separation. This can in turn be inserted into the equation for the vector potential, and the two equations read

$$n_s = 1 + \frac{1}{r} \frac{d}{dr} \left(r \frac{d\gamma_s}{dr} \right), \quad (15)$$

$$\frac{1}{r} \frac{d}{dr} \left(r \frac{da_s}{dr} \right) - \frac{a_s}{\gamma_s^2} \left(\frac{da_s}{dr} \right)^2 + \gamma_s (\kappa \gamma_s - 1) a_s = 0. \quad (16)$$

These equations can be solved numerically in a cylindrical geometry as an eigenvalue problem and it is possible to distinguish between different regimes, depending on the incident power or, in other words, on the parameter κ (the wave-number shift) since there is a direct correspondence between these two quantities. For low-incident powers there is no cavitation structure, only electron-density perturbations [1,2]. Increasing the incident power or equivalently, considering smaller values of κ , the perturbation of the electron density becomes stronger and stronger, the hole in the electron density deeper and deeper, until the minimum electron density vanishes for κ equal to the critical value $\kappa_{cr} = 0.88$ [1]. The power at this point just slightly exceeds the critical one for self-focusing, $P(\kappa_{cr}) = 1.09P_{cr}$. Exceeding this limit, we will have a region depleted of its electrons, $n(r) = 0$. In a stationary regime, the width of such a region is determined by the balance between the pushing ponderomotive force and the restoring force due to the charge-density perturbations. The starting point must be total charge conservation, which in the presence of one cavitation channel ex-

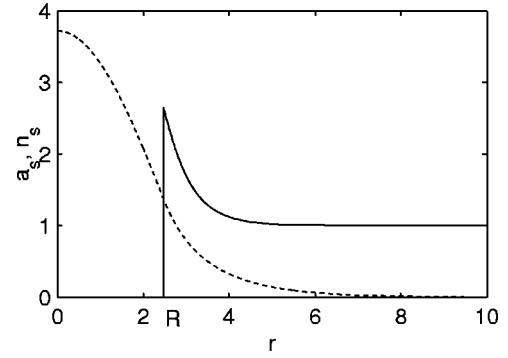


FIG. 1. Stationary single-cavitation structure with $\kappa = 0.5 < \kappa_{cr}$: electron density (solid line) and field (dash line) distributions. No cavitation regions appear for κ larger than the critical value.

tending from the central axis to a certain unknown boundary position R , see Fig. 1, can be written as

$$\int_0^{+\infty} (1 - n_s) r dr = \int_0^R r dr + \int_R^{+\infty} (1 - n_s) r dr = 0. \quad (17)$$

Equation (15) determines the electron-density profile taking into account the two counteracting forces, and therefore, making use of this equation we obtain

$$\left[\frac{a_s a'_s}{\sqrt{1 + a_s^2}} \right]_{r=R} = -\frac{1}{2} R. \quad (18)$$

In order to calculate R , we need to know the values of the field amplitude and its first derivative at $r = R$. Starting from the point R and considering the region $r > R$ we have a plasma field structure which cannot be calculated analytically, but for $0 < r < R$, in the depleted channel, we can write an explicit solution for the field as Eq. (16) reduces to the linear equation

$$\frac{1}{r} \frac{d}{dr} \left(r \frac{da_s}{dr} \right) + \kappa a_s = 0. \quad (19)$$

Therefore, in the cavitation channel the stationary solution for the field is given by a Bessel function of order zero

$$a_s(r) = A J_0(\sqrt{\kappa} r), \quad (20)$$

where A is the amplitude at $r = 0$ (which is not known). At the boundary R , however, we have one more condition to apply, that is the continuity condition for the field and its first derivative

$$a_s(R) = A J_0(\sqrt{\kappa} R), \quad (21)$$

$$a'_s(R) = -A \sqrt{\kappa} J_1(\sqrt{\kappa} R), \quad (22)$$

which can be inserted into Eq. (18) to give the field amplitude as a function of R and κ

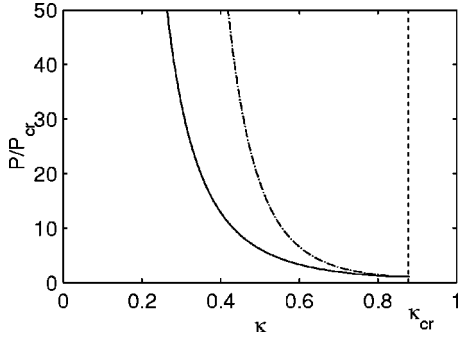


FIG. 2. Total power required to generate one central cavitation channel as a function of the parameter κ calculated without taking into account total charge conservation (dash-dotted line) and with total charge conservation (solid line).

$$A^2 = \frac{R^2}{8\kappa J_1^2(\sqrt{\kappa}R)} \left(1 + \sqrt{1 + \frac{16\kappa J_1^2(\sqrt{\kappa}R)}{R^2 J_0^2(\sqrt{\kappa}R)}} \right). \quad (23)$$

Given a certain κ , for a fixed value of R we know both $a_s(R)$ and $a'_s(R)$. The equation for $r > R$ can be then solved numerically with the shooting method with R as the shooting parameter, in order to find a localized solution with the asymptotic behavior $a_s, a'_s \rightarrow 0$ as $r \rightarrow \infty$. Figure 1 shows one example of such a structure for $\kappa = 0.5 < \kappa_{cr}$.

Furthermore, the power required to generate these configurations can be computed as $P = \int_0^{+\infty} a_s^2 r dr$ and will be a function of the parameter κ . For $\kappa = \kappa_{cr}$ we have an exact estimate of the threshold power for cavitation, in agreement with previous calculations, but as soon as cavitation comes into play, it is evident that previous calculations tend to overestimate the total power. This is due to the fact that, without carefully taking into account charge conservation, an excess of negative charges is present which leads to a higher power being required in order to sustain such structures against the restoring force which is overestimated as a direct consequence of the negative charge excess. If the total charge is conserved, the power needed to generate one central cavitation channel is lower than previously found [1,3,9]. The comparison between our calculations and previous ones is shown in Fig. 2, where laser power is presented in units of the critical power for self-focusing.

It should also be noted that within the framework of Eqs. (11)–(14), the total charge Q is a free parameter. By using the procedure applied above for $Q = 0$, which corresponds to quasineutral plasma guiding structures, it is easy to extend these solutions to any given Q . Such structures with a given net charge over the transverse plane can, in principle, be realized within a restricted space interval but with the global quasineutrality condition defined over the whole space.

B. Plasma filament surrounded by field

Here we would like to emphasize another peculiarity of Eqs. (11)–(14). Structures with a central cavitation channel are not the only possible ones. Another possibility is that of a central electron filament surrounded by a depleted ring centered on the axis. The character of this kind of configuration

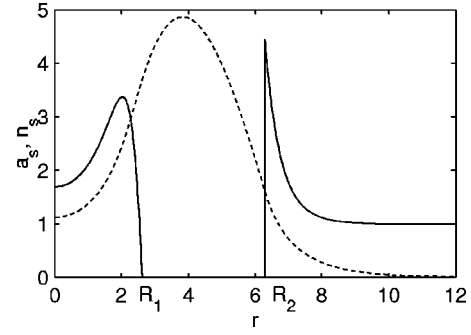


FIG. 3. Stationary filament structure with zero electron density at the filament boundary R_1 (i.e., the free parameter is defined only by the requirement of the existence of a localized solution) for $\kappa = 0.3$: electron density (solid line) and field (dash line) distributions.

depends on the incident power. Such structures do not exist at low-power levels and their existence is connected with the cavitation phenomenon and thus it has a power threshold for excitation. The procedure to calculate the plasma field structures for this case starts from the central axis. With the shooting method the field distribution and electron-density distribution for the central electron filament can be calculated. In this case, the on-axis value of the field will act as a shooting parameter, while its first derivative must be zero on axis due to the symmetry of the configuration. Thus we have a certain freedom when choosing the boundary position of this channel R_1 , see Fig. 3, the only requirement being, so far, that the electron density must not be negative. The minimum incident power for generating such a structure at a fixed κ is such that the electron density at R_1 vanishes, which is the case presented in Fig. 3 (solid line) (but, of course, this is not a unique choice for finding localized solution as we will see below). Once a choice of R_1 has been made, we know the amplitude and the first derivative of the field at this point, $a_s(R_1)$, $a'_s(R_1)$, and we can make use of the matching conditions to determine the parameters of the vacuum solution, which is a superposition of the zeroth-order Bessel and Neumann functions, i.e.,

$$a_s(r) = A_v J_0(\sqrt{\kappa}r) + B_v Y_0(\sqrt{\kappa}r). \quad (24)$$

This solution describes the field in the cavitation region, which extends from R_1 to a still unknown position R_2 . In particular we have

$$a_s(R_1) = A_v J_0(\sqrt{\kappa}R_1) + B_v Y_0(\sqrt{\kappa}R_1), \quad (25)$$

$$a'_s(R_1) = -A_v J_1(\sqrt{\kappa}R_1) - B_v \sqrt{\kappa} Y_1(\sqrt{\kappa}R_1). \quad (26)$$

It is then the constraint of total charge conservation that dictates how far the cavitation channel can extend. Inserting Poisson's equation and the force balance equation into the total charge conservation law

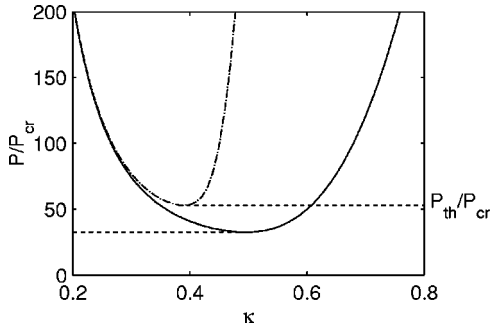


FIG. 4. Total power for the case of the filament structure in Fig. 3 as a function of the parameter κ . The solid line represents the minimum laser power needed to sustain a filament mode with zero density at R_1 , while the dash lines correspond to $n_s(R_1)=2.4$.

$$\int_0^{+\infty} (1-n_s)rdr = \int_0^{R_1} (1-n_s)rdr + \int_{R_1}^{R_2} rdr + \int_{R_2}^{+\infty} (1-n_s)rdr = 0 \quad (27)$$

and taking into account the symmetry of the configuration and the asymptotic behavior of the localized solution we are looking for, a relation between R_1 and R_2 is established, viz.

$$g(R_1) - g(R_2) = \frac{1}{2}(R_2^2 - R_1^2), \quad (28)$$

where

$$g(r) = \frac{ra_s a'_s}{\sqrt{1+a_s^2}}. \quad (29)$$

Once R_2 has been calculated, what is left is to check that the solution in the last semi-infinite plasma region is actually a localized solution. An example of such a structure is presented in Fig. 3 and the related power as a function of κ is shown in Fig. 4 (solid line).

As for the choice of the left boundary position R_1 we have a certain freedom. In fact for a given propagation constant κ , the solution is not unique, rather there is a continuous family of such solutions within a certain power range, as clearly seen in Fig. 4 where the minimum power that can sustain such structures as a function of κ is presented. For increasing boundary density, the power needed to sustain such structures increases too. However, formally in the limiting case at fixed κ , the maximum power goes to infinity. As an example, in Fig. 4 we also present the power dependence on κ for the filament boundary density $n_s(R_1)=2.4$. As we will see below, this curve separates stable and unstable filament structures. Such configurations can be generated by a laser beam with a minimum intensity on axis and present the interesting feature of strong filament density perturbations, so that the actual electron density in the filament can reach values significantly higher than the unperturbed one. The growing behavior of the maximum density values in the filament as a

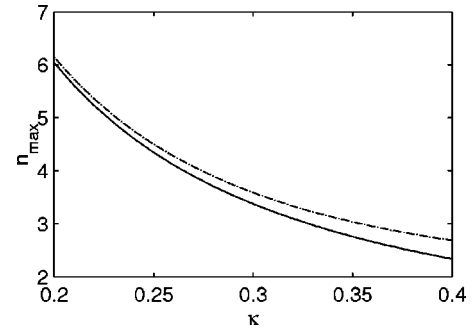


FIG. 5. Maximum density values in the filaments as a function of the parameter κ . The dashed and solid lines correspond to curves in Fig. 4.

function of κ is shown in Fig. 5, while Fig. 6 shows how the boundary positions R_1 and R_2 depend on the parameter κ . As clearly seen from Fig. 4, with this kind of configuration the power is not uniquely related to κ and, in fact, two qualitatively different branches are possible. These two branches are characterized by strong [left branches from the minimum of the curve at fixed $n_s(R_1)$] or weak (right branch with power increasing with κ) density perturbations. We note that the left branch solutions represent a new type of structure, whereas the right branch may be rather considered as a generalization of the one-dimensional single-cavity structure to cylindrical geometry with the localized structure lying far from the axis as seen in Fig. 6. Usually the latter are unstable not only with exponentially growing symmetry-breaking perturbations but also with linearly growing perturbations: in this case, it tends to compress the ring since opposite parts attract each other. It should also be emphasized that these cavitation structures can be produced only if the power exceeds some minimal level equal to $33.4P_{cr}$, but for the stable structures (as shown below for the case of Fig. 4) $P > P_{th} = 53P_{cr}$. In this sense, P_{th} assumes the role of threshold power for generation of such stable filament structures. These plasma structures may be of interest for the x-ray laser problem since they represent long plasma filaments with high densities supported by strong laser fields.

C. Self-focusing ring structures

It is also possible to find solutions with more than one cavity that can support so-called ring structures of laser ra-

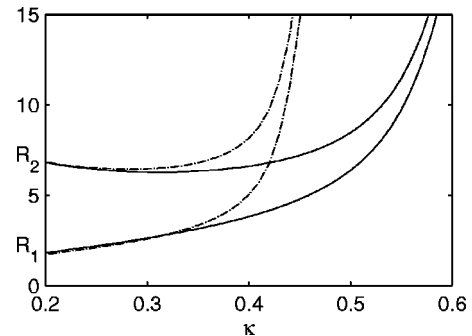


FIG. 6. Boundary positions R_1 and R_2 for the filament structures as functions of the parameter κ . The dashed and solid lines correspond to curves in Fig. 4.

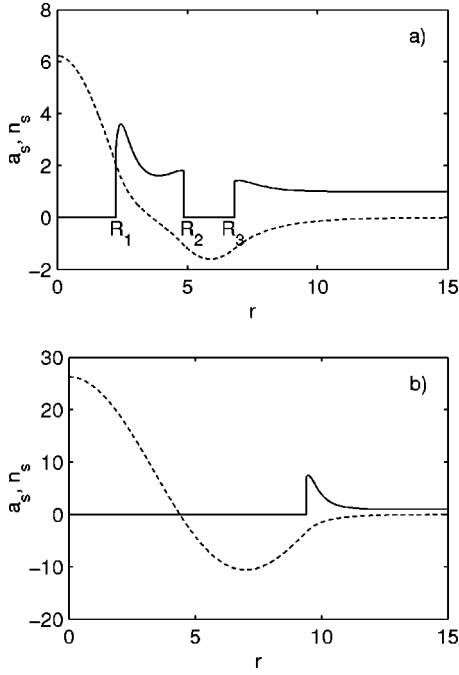


FIG. 7. Two-cavity structure (a) with the field passing through zero for $\kappa=0.6$ and $n_s(R_1)=2.7$, $n_s(R_2)=1.8$; (b) the limit case, for increasing power, of the two-cavity structure for the same κ as for a single cavity: electron density (solid line) and field (dash line) distributions.

diation. At first instance, these structures might be treated as higher-order nonlinear modes [3,8] and considered as a continuation of higher-order solutions of the nonlinear Schrödinger equation [14], which is valid for the present problem in the weakly relativistic limit. However, as was shown by Kolokolov and Sukov [16], all higher-order modes in media with local nonlinearity are unstable and, therefore, do not represent a situation of practical interest. For higher intensities, regions with decreased electron density will be transformed into depletion regions. This implies that the cavitation regime corresponds to an extremely saturated nonlinearity, which, in fact, can be stable as shown below. Because of this, we have considered these structures in some more detail. Some of these solutions, with a denumerable number of cavities and qualitatively corresponding to the one-dimensional case, are presented in [12]. Obviously, not all of these structures can appear in an axisymmetric geometry due to the requirement of symmetry. Moreover, the procedure of constructing these solutions for the axisymmetric case is more complex as compared with the case of the one-dimensional geometry, even numerically. The procedure is as follows. In the central cavity $r < R_1$ [see Figs. 7(a) or 8], the solution for the field is of the form given by Eq. (20), where at fixed amplitude A (the shooting parameter), the field value and its first derivative are known. Integrating Eqs. (11)–(14) over the nearest plasma layer lying within the interval $R_1 \leq r \leq R_2$, we arrive at the boundary R_2 having two degrees of freedom: the choice of the values of R_1 and R_2 is restricted only by the requirements that the electron-density function should be positive. However, the actual value can vary from zero to some value defined by the existence of a localized

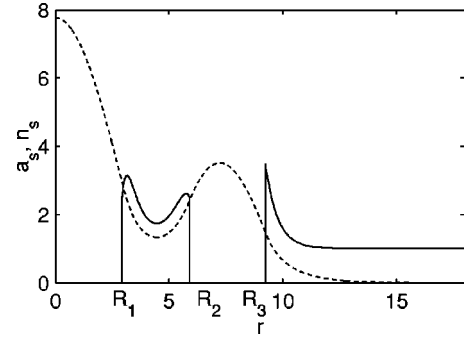


FIG. 8. Two-cavity structure without sign reversed field for $\kappa=0.35$ and $n_s(R_1)=2.5$, $n_s(R_2)=2.5$: electron density (solid line) and field structure (dash line).

solution. In the next cavity region ($R_2 < r < R_3$), integrating Poisson's equation over the whole interval and taking into account the fact that the net charge must equal zero, we arrive at the transcendental equation

$$\sum_{i=1}^3 (-1)^i \left[\frac{1}{2} R_i^2 + g(R_i) \right] = 0 \quad (30)$$

where the function $g(r)$ obeys Eq. (29). This equation, being a generalization of Eqs. (18) and (28) to the case of a higher number of cavities, defines the boundary position R_3 together with the corresponding field amplitude and its derivative for given R_1 and R_2 . After this, integrating again Eqs. (11)–(14) over the semi-infinite plasma layer ($R_3 \leq r < \infty$), while requiring a localized solution, we obtain the total plasma-field structure. There are two continuous families of such two-parametric [$n_s(R_1)$ and $n_s(R_2)$] solutions with the corresponding laser power uniquely defined for fixed κ . Figure 7(a) shows an example of the first one with the field passing through zero. This may be considered as a generalization, to higher-incident laser powers, of the higher-order modes of the nonlinear Schrödinger equation to the cavitation regime. The cavity widths (R_1 and $R_3 - R_2$) and the electron layer width ($R_2 - R_1$) are comparable with κ^{-1} over a broad range of laser powers, but for increasing power, the electron width decreases to zero. Thus, in this limit the two-cavity structure will transform into a single-cavity structure, but will contain a vacuum field distribution passing through zero, as shown in Fig. 7(b). Since this problem is multiparametric and too complex to be presented in a simple way, we also, as an example, present in Fig. 9 (dash-dotted line) the power dependence on κ for fixed electron densities at the boundaries: $n_s(R_1)=2.7$ and $n_s(R_2)=1.8$.

The second family of solutions without sign reversed field distributions represents a type of solution that exists only in the cavitation regime. As an example, in Fig. 8 is shown the solution for $\kappa=0.35$ and $n_s(R_1)=2.5$, $n_s(R_2)=2.5$. The dependence of power on κ for fixed boundary parameters is shown in Fig. 9 (solid line). We note that for these structures, similarly to the filament solutions, the power versus κ can have two meanings, which corresponds to two different branches: in the first one (left branch from the minimum of the curve), the widths of the cavities and the electron layers

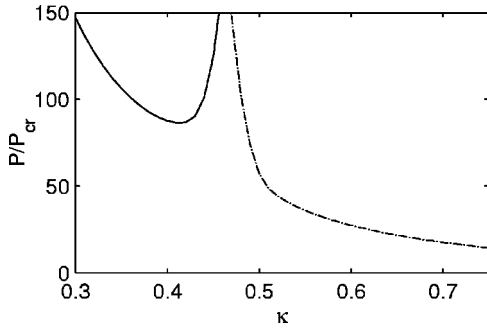


FIG. 9. The power of the two-cavity structures as a function of κ for fixed electron density at the boundaries: without sign reversed field at $n_s(R_1)=2.5$, $n_s(R_2)=2.5$ (solid line); with field passing through zero at $n_s(R_1)=2.7$, $n_s(R_2)=1.8$ (dash-dotted line).

are of the order of κ^{-1} ; in the second (right) branch, for increasing power, the width of the electron layer (or the boundary position R_2) increases. Thus, finally the two-cavity solution may be considered as a superposition of a single-cavity structure and a one-dimensional one-cavity structure lying far from the axis. The procedure of calculating structures with more than two cavities is the same, but with the difference that it introduces more free parameters (one for each additional cavity) and consequently other terms will appear in Eq. (30).

IV. STRUCTURAL STABILITY

Strictly speaking, an analysis of the nonlinear stability as well as of the evolution of the relativistic self-focusing in the cavitation regime cannot be done within the framework of Eqs. (7)–(10) since the boundaries of the cavities cannot be determined self consistently from global charge conservation. However, if the plasma-field distributions of the stationary structures are known (see Sec. III), we are able, by using Eqs. (7)–(10), to study the problem of structural stability assuming exponentially growing small perturbations. For this purpose we assume $a=[a_s(r)+a_1(\mathbf{r},z)]e^{-i\kappa z}$, $n=n_s(r)+n_1(\mathbf{r},z)$ where a_s , n_s are the stationary solutions of Eqs. (11)–(14), and a_1 , n_1 are small perturbations. Substituting this ansatz into Eqs. (7)–(10), the growth rate of the small perturbations (a_1 and $n_1 \propto e^{\Gamma z}$) is determined by the eigenvalue problem:

$$\widehat{L}_0 v(\mathbf{r}) = \Gamma u(\mathbf{r}), \quad (31)$$

$$\widehat{L}_1 u(\mathbf{r}) = -\Gamma v(\mathbf{r}), \quad (32)$$

where $a_1 = u + iv$, u and v are the real functions, and the operators \widehat{L}_0 and \widehat{L}_1 are given by ($\gamma_s = \sqrt{1+a_s^2}$)

$$\widehat{L}_0 = -\nabla^2 - \kappa + \frac{n_s}{\gamma_s}, \quad (33)$$

$$\widehat{L}_1 = \widehat{L}_0 - \frac{n_s a_s^2}{\gamma_s^3} + \frac{a_s}{\gamma_s} \nabla^2 \frac{a_s}{\gamma_s}. \quad (34)$$

In the cavitation regions where $n_s(r)=0$, the operators \widehat{L}_1 and \widehat{L}_0 coincide: $\widehat{L}_1 = \widehat{L}_0 = -\nabla^2 - \kappa$ and on the boundaries of the electron layers, the functions u , v , and their first derivatives are continuous.

We emphasize that in spite of the fact that the cavity structures are determined by differential equations of higher than the second order (for example, in the one-dimensional case with different Hamiltonian values from layer to layer [12]), nevertheless the eigenvalue problem is similar to the case of local nonlinearity [15–18]. However, the second-order operators \widehat{L}_0 , \widehat{L}_1 here have effective step-wise potentials where the cavity boundaries are fixed. From this point of view, it is convenient to review some common properties of the set of Eqs. (31) and (32) that will be useful in order to draw some qualitative conclusions. All the stationary solutions $a_s(r)$ with corresponding density distributions $n_s(r)$, are eigenfunctions of the operator L_0 with the eigenvalues equal to zero as follows from Eq. (11). For the two most important cases, single channeling and a plasma filament surrounded by field, they correspond to the lowest eigenfunctions that do not pass through zero. This implies that all higher-order eigenfunctions have positive eigenvalues. We also note that by using Eq. (31) we obtain $\langle u | a_s \rangle = 0$, where $\langle a | b \rangle = \int a b^* ds$, and therefore the subspace of the solutions of Eqs. (31) and (32) with $\Gamma \neq 0$ is orthogonal to the ground state a_s . In this subspace of functions, the operator \widehat{L}_0 is positive definite, thus assuring the existence of the inverse operator \widehat{L}_0^{-1} . Combining Eqs. (31) and (32) into one and applying the inverse operator we arrive at the following expression defining the eigenvalue:

$$\Gamma^2 = - \frac{\langle u | \widehat{L}_1 u \rangle}{\langle u | \widehat{L}_0^{-1} u \rangle}. \quad (35)$$

As follows from this equation, since the operator \widehat{L}_0^{-1} is also positive definite, the stability problem depends on the properties of the operator \widehat{L}_1 . In accordance with the theory developed by Kolokolov and Vakhitov [15], if the operator \widehat{L}_1 admits only one negative eigenvalue, the ground state is stable when the power is a decreasing function of the propagation constant, i.e., $\delta P / \delta \kappa < 0$, the so called Vakhitov and Kolokolov criterion, otherwise it is unstable. If the operator \widehat{L}_1 has more than one negative eigenvalue, the ground state is unstable. In order to solve numerically the eigenvalue problem, it is convenient to rewrite Eqs. (31) and (32) in the following form:

$$\widehat{L}_0 v(\mathbf{r}) = \Gamma u(\mathbf{r}), \quad (36)$$

$$\widehat{L}_1 u(\mathbf{r}) = -\gamma_s^2 \Gamma v(\mathbf{r}), \quad (37)$$

where the operator \widehat{L}_1 is written in the same structural form as \widehat{L}_0 :

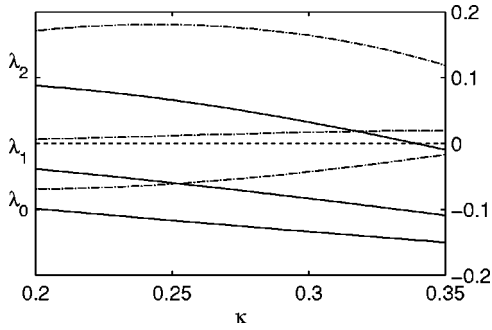


FIG. 10. Eigenvalues λ_m of the operator \widehat{L}_1 as a function of κ for the filament structure with $n_s(R_1)=0$ (solid lines) and $n_s(R_1)=3.0 > n_s^*$ (dash-dotted lines) for different azimuthal indexes ($m=0,1,2$).

$$\widehat{L}_1 = -\nabla^2 + \frac{\nabla a_s^2}{\gamma_s^2} \nabla - \kappa + \frac{\widetilde{n}_s}{\gamma_s}, \quad (38)$$

$$\widetilde{n}_s = n_s + a_s^2 \left[1 - 2\kappa\gamma_s - \frac{2(\nabla a_s)^2}{\gamma_s^3} \right]. \quad (39)$$

Since in Eq. (37) γ_s^2 is a positive definite function, conclusion about the stability problem may be drawn from the operator \widehat{L}_1 as well. It is also useful to know the eigenvalue problem for \widehat{L}_1 : $\widehat{L}_1 \psi_m = \lambda_m \psi_m$ (where m is the azimuthal index, λ_m and ψ_m are the eigenvalue and eigenfunction, respectively) since the general problem of finding the eigenfunctions of Eqs. (36) and (37) is a formidable task even computationally. This knowledge also essentially simplifies the numerical search of these solutions.

A. Stable single-channel wave guiding

For the single-channel solutions considered in Sec. III A, the operator \widehat{L}_1 admits only one negative eigenvalue corresponding to azimuthal index $m=0$, all the others with higher azimuthal indices are positive. Therefore, stability of these stationary structures can be analyzed by the Vakhitov and Kolokolov criterion. For the main axisymmetric modes, the dependence of power on the propagation constant presented in Fig. 2 meets the stability criterion, thus proving the stability of single-channel wave guiding.

B. Stability of filament structure

For a case when a plasma filament is surrounded by a bright ring beam (see Sec. III B), the operator \widehat{L}_1 can have several negative eigenvalues as shown in Fig. 10, corresponding to symmetric (azimuthal index $m=0$) and different asymmetric eigenfunctions ($m=1,2$). Since in this case the amplitude distribution $a_s(r)$ never passes through zero as for the single channel case (see Fig. 1), we can again apply the stability criterion of Vakhitov and Kolokolov by considering the power dependence versus κ for fixed boundary parameter, however only for symmetrical perturbations (see, for

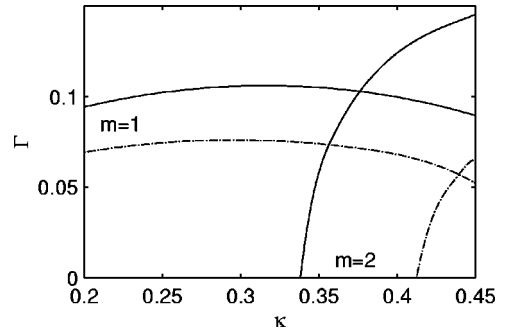


FIG. 11. The growth rate for $m=1,2$ as a function of κ for the filament structures as in Fig. (4): solid lines correspond to the minimum power curve, while dash-dotted lines correspond to a power curve with $n_s(R_1)=1.0 < n_s^*$.

example, [17]). According to this criterion, the right-hand branches in Fig. 4 (right from the minimum) correspond to unstable structures. However, for the structures corresponding to the left-hand branch, the problem of stability is not clear (although they are stable against symmetrical perturbations) because the operator \widehat{L}_1 may also admit negative eigenvalues for asymmetric eigenfunctions. For example, for the curve with the minimum laser power [Fig. 4 (solid line)], \widehat{L}_1 has at least two negative eigenvalues in the whole interval of κ , as seen in Fig. 10 (solid lines), and therefore these structures are unstable. For increasing boundary density, $n_s(R_1)$, we arrive at the case when $\lambda_1=0$. In this case we found that $n_s(R_1)=n_s^* \approx 2.45$ in the whole interval of κ for the left-hand branch. At slightly higher density values, the typical dependence of the eigenvalues on κ is shown in Fig. 10 (dash-dotted lines). Consequently, the left-hand branch of the dash-dotted line in Fig. 4 separates stable and unstable filament structures and the minimum of this curve corresponds to a real threshold power for generating such structures. In the general case we have to solve Eqs. (36) and (37) directly and this was done numerically for the eigenvalue problem, noting that the solutions in the vicinity of the axis vary as $u, v \sim r^m$ and that the asymptotic behavior at infinity ($r \rightarrow \infty$) is known. In Fig. 11 the dependence of the growth rate Γ on κ is presented for $m=1,2$. As we see, the field structures corresponding to the curve with the minimum power in Fig. 4 are always unstable. The increment has an absolute maximum for the eigenfunction with $m=2$ but it is localized in a more narrow region of κ . At increasing boundary density, the growth rate becomes smaller and smaller [as seen in Fig. 11, for example, at $n_s(R_1)=1.0$] implying that filament structures lying above the threshold power curve corresponding to $n_s(R_1)=n_s^*=2.4$ are stable. Thus, at high laser power we can expect the creation of stable laser-plasma structures.

C. Stability of ring structures

The stability of ring structures presented in Sec. III C is not quite clear. In media with local nonlinearities, such solutions are always unstable [16,17], usually being destroyed by

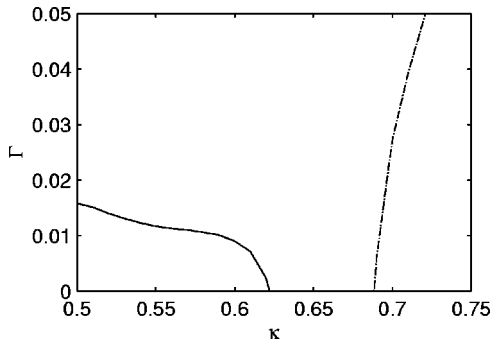


FIG. 12. The growth rate as a function of κ for the two-cavity structures in Fig. 9 (dash-dotted line): $m=1$ (solid line) and $m=2$ (dash-dotted line).

perturbations which break the azimuthal symmetry of the beams. However, in the present problem, the cavitation regions tend to become larger at higher-laser power. This implies that the contribution of the nonlinear part, which is responsible for the instability, becomes smaller compared with the cavitation (“vacuum”) part. Therefore, we can expect the existence of structures which are stable against small perturbations. In order to solve this problem directly we can use a two-step approach: first, to solve the eigenvalue problem for the operator \widehat{L}_1 and then, having information about the possible range of growth rates, to solve the full problem given by Eqs. (36) and (37). Since the ring structures depend on many parameters, we present different examples demonstrating the stability for some of them. Figure 12 represents the growth rates corresponding to the structures in Fig. 9. Unstable as well as stable solutions are clearly seen. There is a gap in the interval $0.62 < \kappa < 0.68$ between the growth rates for azimuthal modes with $m=1$ and $m=2$ (and also all higher modes with $m > 2$) with increments equal to zero (with nonzero growth rates they lie to the right of the case $m=2$). This means that structures with parameters within this gap are stable. We note that all the structures existing in the form of one cavity while the second one contains only a density variation are always unstable. Consequently, in order to have stability of the plasma-field structures they must be in the form of a cavity emptied of electrons. The results of the calculations can be summarized as follows: the stability of the structures is most sensitive to the last layer density

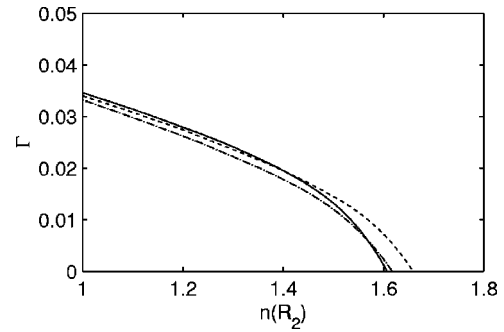


FIG. 13. Dependence of the growth rate for $m=1$ on $n_s(R_2)$ for the two-cavity structures for fixed $\kappa=0.65$ and $n_s(R_1)=0$ (solid line), 1.0 (dash-dotted line), 2.7 (dashed line).

level $[n_s(R_2)]$ and less sensitive to the parameters of the previous electron layers. This is clearly seen in Fig. 13 where the growth rates presented for fixed propagation constant only weakly depend on $n_s(R_1)$ but strongly depend on $n_s(R_2)$ decreasing with increasing $n_s(R_2)$. It should be noted that higher-boundary density levels can be sustained with higher powers. Furthermore, if such structures for fixed $n_s(R_1)$ and $n_s(R_2)$ are supported by lower-laser power levels (depending on κ) they have enhanced stability. The main conclusion is that stable two-cavity structures can indeed be produced in laser-plasma interactions.

V. CONCLUSION

In this paper, we have shown how it is possible to extend the stationary solution describing cavitation structures due to self-focusing and self-channeling of superintense laser pulses in underdense plasmas with axial symmetry, to a description that fully takes into account plasma quasineutrality. The rigorous conservation of global charge leads to an estimate of the power necessary to generate such structures. If the critical power for cavitation is correctly estimated, the power to generate such structures with strong density perturbations turns out to be lower than previously found. Stationary configurations with one central cavitation channel as well as with a cylindrical cavitation ring have been presented. The problem of stability has been also considered showing that stable formation of such structures is possible.

-
- [1] G. Z. Sun *et al.*, Phys. Fluids **30**, 526 (1987).
 [2] T. Kurki-Suonio, P. J. Morrison, and T. Tajima, Phys. Rev. A **40**, 3230 (1989).
 [3] A. B. Borisov *et al.*, Phys. Rev. A **45**, 5830 (1992).
 [4] B. Hafizi *et al.*, Phys. Rev. E **62**, 4120 (2000).
 [5] M. Tabak *et al.*, Phys. Plasmas **1**, 1626 (1994).
 [6] M. D. Feit *et al.*, Phys. Rev. E **56**, R2394 (1997).
 [7] M. Borghesi *et al.*, Phys. Rev. Lett. **78**, 879 (1997); K. A. Tanaka *et al.*, Phys. Rev. E **62**, 2672 (2000).
 [8] A. B. Borisov *et al.*, Plasma Phys. Controlled Fusion **37**, 569 (1995).
 [9] A. M. Komashko *et al.*, Pis'ma Zh. Éksp. Teor. Fiz. **62**, 849 (1995) [JETP Lett. **62**, 860 (1995)].
 [10] M. D. Feit *et al.*, Phys. Rev. E **57**, 7122 (1998).
 [11] A. G. Litvak, Zh. Éksp. Teor. Fiz. **57**, 629 (1969) [Sov. Phys. JETP **30**, 344 (1970)]; C. Max, J. Arons, and A. Langdon, Phys. Rev. Lett. **33**, 209 (1974).
 [12] F. Cattani *et al.*, Phys. Rev. E **64**, 016412 (2001).
 [13] X. L. Chen and R. N. Sudan, Phys. Fluids B **5**, 1336 (1993).
 [14] H. A. Haus, Phys. Lett. **8**, 128 (1966); Z. K. Yankauskas, Izv.

- Vuz. Radoifiz. **9**, 412 (1966) [Radiophys. Quantum Electron **9**, 261 (1968)].
- [15] N. G. Vakhitov and A. A. Kolokolov, *Izv. Vuz. Radoifiz.* **16**, 1020 (1973) [Radiophys. Quantum Electron **16**, 783 (1975)].
- [16] A. A. Kolokolov and A. I. Sykov, *Zh. Prikl. Mekh. Fiz.* **4**, 55 (1975) [*J. Appl. Mech. Tech. Phys.* **4**, 519 (1975)]; J. M. Soto-Crespo *et al.*, *Phys. Rev. A* **44**, 636 (1991).
- [17] J. Atai, Y. Chen, and J. M. Soto-Crespo, *Phys. Rev. A* **49**, R3170 (1994).
- [18] V. Zakharov, S. Musher, and A. Rubenchik, *Phys. Rep.* **129**, 285 (1985).